40. Shimura H, Schlossmacher MG, Hattori N, Frosch MP, Trockenbacher A, Schneider R, Mizuno Y, Kosik KS, Selkoe DJ: Ubiquitination of a new form of α-synuclein by parkin from human brain: implications for Parkinson's disease. Science 2001, 293:263–269
41. Kitada T, Asakawa S, Hattori N, Matsumine H, Yamamura Y, Minoshima S, Yokochi M, Mizuno Y, Shimizu N: Mutations in the parkin gene cause autosomal recessive juvenile parkinsonism. Nature 1998, 392:605–608
42. Shimura H, Hattori N, Kubo S, Mizuno Y, Asakawa S, Minoshima S, Shimizu N, Iwai K, Chiba T, Tanaka K, Suzuki T: Familial Parkinson disease gene product, parkin, is a ubiquitin-protein ligase. Nat Genet 2000, 25:302–305
43. Imai Y, Soda M, Takahashi R: Parkin suppresses unfolded protein stress-induced cell death through its E3 ubiquitin-protein ligase activity. J Biol Chem 2000, 275:35661–35664
44. Zhang Y, Gao J, Chung KK, Huang H, Dawson VL, Dawson TM: Parkin functions as an E2-dependent ubiquitin-protein ligase and promotes the degradation of the synaptic vesicle-associated protein, CDCrel-1. Proc Natl Acad Sci USA 2000, 97:13354–13359
45. Chung KK, Zhang Y, Lim KL, Tanaka Y, Huang H, Gao J, Ross CA, Dawson VL, Dawson TM: Parkin ubiquitinates the α-synuclein-interacting protein, synphilin-1: implications for Lewy-body formation in Parkinson disease. Nat Med 2001, 7:1144–1150
46. Bence NF, Sampat RM, Kopito RR: Impairment of the ubiquitin-proteasome system by protein aggregation. Science 2001, 292: 1552–1555
47. Okochi M, Walter J, Koyama A, Nakajo S, Baba M, Iwatsubo T, Meijer L, Kahle PJ, Haass C: Constitutive phosphorylation of the Parkinson's disease associated α-synuclein. J Biol Chem 2000, 275: 390–397
48. Fujiwara H, Hasegawa M, Dohmae N, Kawashima A, Masliah E, Goldberg MS, Shen J, Takio K, Iwatsubo T: α-Synuclein is phosphorylated in synucleinopathy lesions. Nat Cell Biol 2002, 4:160–164

SHORT REPORT

Sjögren's syndrome associated painful sensory neuropathy without sensory ataxia

K Mori, M Iijima, M Sugiura, H Koike, N Hattori, H Ito, M Hirayama, G Sobue

J Neurol Neurosurg Psychiatry 2003;74:1320–1322

Sensory neuropathy with prominent ataxia reflecting kinesthetic sensory impairment is a well recognised form of neuropathy associated with Sjögren's syndrome.[1-4] Pathologically, T cell invasion of dorsal root ganglia, loss of large sensory neurons, and secondary large fibre degeneration is seen in this neuropathy.[4] However, a form of neuropathy associated with Sjögren's syndrome, presenting with pain and superficial sensory involvement without sensory ataxia has been described anecdotally[5] and in a case report.[6] Clinicopathological details of the second form of neuropathy have not been elucidated. In this report we describe seven patients with Sjögren's syndrome showing painful sensory neuropathy without sensory ataxia.

Patients studied were referred for painful neuropathy to Nagoya University Hospital and its affiliated institutions. All seven patients fulfilled diagnostic criteria for Sjögren's syndrome by the American-European Consensus Group[7] and showed painful peripheral neuropathy (table 1). Patients included six women and one man, ranging from 25 to 72 years old. In all patients initial symptom of neuropathy was paraesthesia or painful dysaesthesia in the most distal portions of the extremities, later extending proximally to involve the entire legs and arms. The trunk became involved in three patients, and the trigeminal nerve was impaired in three patients. Asymmetry in sensory impairment was present in four patients. None of the patients showed sensory ataxia in the initial phase. Most patients retained essentially normal muscle strength, but patient 1 showed slight weakness in distal limb muscles. Painful sensation was the most characteristic, and this symptom compromised activities of daily living in all patients. Superficial sensation for pinprick and temperature was prominently impaired. Deep sensation such as joint position and vibratory sense was substantially well preserved. Sensory ataxia and Romberg's sign was not seen. Autonomic dysfunction was seen in four patients including Adie's pupils, urinary disturbance, and loss of ^{123}I-MIBG cardiac accumulation; however, orthostatic hypotension was not present. Apparent hypohidrosis was seen in three patients. Thermal stimulation in two patients, resulted in absent sweating on the forehead, trunk, arms, and legs, with preserved sweat gland function on pirocarpine test. Thermography showed abnormal skin temperature gradient in four patients. Deep tendon reflexes were comparatively well preserved except in two patients. Motor nerve conduction studies showed no slowing (mean (SD) 52.3 (3.9) m/s in the median, 44.8 (6.1) m/s in the tibial nerves) and preserved compound muscle action potentials (CMAPs) (7.5 (3.5) mV in the median, 9.0 (6.3) mV in the tibial nerves). Sensory nerve conduction (50.1 (6.0) m/s in the median, 47.2 (10.4) m/s in the sural nerves) and sensory nerve action potentials (SNAPs) (13.6 (11.7) uV in the median and 9.0 (6.3) uV in the sural nerves) were generally well preserved; only in patient 4, SNAPs were not evoked. Somatosensory evoked potentials (SEPs) were also well preserved (mean (SD) 20.0 (1.1) ms at N20, 13.7 (1.2) ms at N13, and 9.3 (0.4) ms at N9).

Sural nerve biopsy in five patients showed a variable degree of myelinated fibre loss, predominantly affecting small diameter fibres (table 1, fig 1). Unmyelinated fibre density also was severely reduced. Axonal sprouting was essentially absent in all patients. In teased fibre preparations, degeneration was seen in 32% to 55% of axons, predominantly small diameter fibres. Vasculitis was not seen.

Patient 2 developed sensory ataxia in the legs over the next nine years, and more details of this patient are given below. Patient 4 developed localised sensory ataxia in the fingers of the right hand over 11 years. Other patients showed persistent painful sensory neuropathy with gradual extension of distribution over 4 to 11 years of follow up.

CASE REPORT

A 68 year old man had painful dysaesthesia and numbness in the feet for about 10 years, with spread to the proximal of the legs and arms. When he was 56 years old, he noticed painful dysaesthesia in the legs, and subsequently in the hands. Neurological examination demonstrated light touch and pinprick were disturbed, and painful dysaesthesia was elicited in glove and stocking distribution. Vibration and joint position sense was comparatively well preserved for the first time. Sensory ataxia and Romberg's sign were not seen. Deep tendon reflexes were well preserved in upper limbs, but mildly decreased in lower limbs. Muscle strength was normal. Autonomic disturbance was not present. Nerve conductions were nearly normal except for sensory conduction in the median nerve, 40 m/s. SNAPs were well preserved. Result of routine blood haematology and biochemistry screening tests were normal. CSF protein was 33 mg/dl with no cells. A sural nerve biopsy specimen revealed myelinated fibre loss predominantly involving small diameter fibres with axonal degeneration.

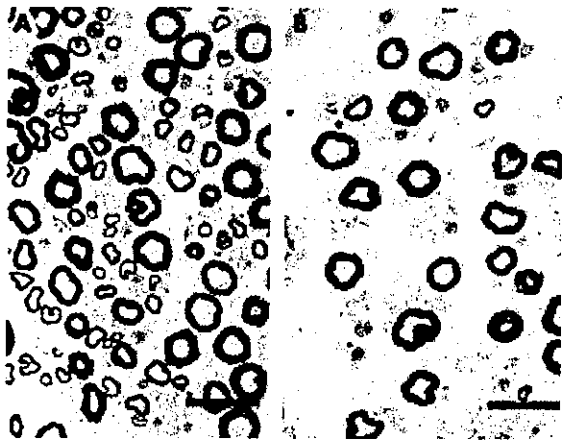

Figure 1 (A) Transverse section of a sural nerve specimen from a control subject. (B) Specimen from a patient of painful sensory neuropathy with predominant small fibre loss associated with Sjögren's syndrome (patient 1). Small diameter myelinated fibres are more noticeably involved and no axonal sprouting. Bars=25 μm.

Table 1 Clinical symptoms and histopathological findings

Patient Age/sex	Sjögren's syndrome, positive test	Neurological symptoms: Motor involvement Muscle atrophy/ strength	Sensory involvement: Distribution	Painful sensation	Nociception	Vibration/ position sense	Sensory ataxia	Romberg's sign	Autonomic signs	Sural nerve biopsy: Myelinated fibre density large, 9 small (no/mm²), Small/large ratio	Unmyelinated fibre density (no/mm²)	Follow up (y)
1 72/F	SS-A SS-B Sialography	+1 / +1	TL	+3	−3	−1 /−	−	−	1, 2, 4	axonal degeneration 1159, 921, 0.79	3463	6
2 68/M	SS-A Lip biopsy RB	−/−	L	+2	−3	−1 / −1	−*	−*	4	axonal degeneration 922, 448, 0.49 79, 169, 2.14‡	ND	2
3 36/F	Lip biopsy RB	−/−	TL	+3	−3	−/−	−	−	3	axonal degeneration 1876, 1332, 0.71	2585	6
4 71/F	SS-A Sialography RB	+1 /−	L	+3	−3	−2 / −2	−†	−	1, 2, 4	axonal degeneration 1158, 1553, 1.34	8312	11
5 48/F	Lip biopsy Gum test	−/−	FL	+3	−3	−/−	−	−	−	axonal degeneration 2541, 1528, 0.62	3232	11
6 25/F	SS-A RB	−/−	FL	+3	−3	−/−	−	−	1	ND	ND	6
7 62/F	Lip biopsy Schirmer's test	−/−	FL	+3	−3	−/−	−	−	−	ND	ND	4
Controls (mean (SD), n=9)									3068 (294),	5122 (438), 1.7 (0.2)	29913 (3457)	

+, Positive findings; −, negative findings. Muscle weakness, atrophy, and painful sensation: +3, severe; +2, moderate; +1, mild; −, absent. Distribution of sensory involvement: F, facial; T, trunk; L, limbs. Sensory signs: −3, severe; −2, moderate; −1, mild; −, absent. Nociception was evaluated by pin pricking. Autonomic dysfunction: 1, Adie's pupils; 2, loss of ^{123}I-MIBG cardiac accumulation; 3, urinary disturbance; 4, hypohidrosis. SS-A, anti-SS-A antibody; SS-B, anti-SS-B antibody; RB, Rose Bengal test for Sjögren's syndrome. For nerve biopsy findings, large >6.73 um; small <6.73 μm in fibre diameter; As for typical sensory ataxic neuropathy with Sjögren's syndrome, large myelinated fibre density was 660 (714) (mean (SD)), small myelinated fibre density was 3263 (2390), and small/large fibre ratio was 14.6 (19.0) for 20 cases. ND, not determined. *,†Sensory ataxia developed in the legs 9 years later, in the right hand 11 years later respectively. ‡Result of second sural nerve biopsy examined 12 years later.

In the next nine years, involvement of deep sensation gradually developed. At 68 years old, he showed sensory ataxia in the legs and positive Romberg's sign without muscle weakness. The deep tendon reflexes were almost absent. Motor nerve conduction velocities were still preserved, but sensory nerve action potentials were not elicited in the median and sural nerves. At this time, sicca symptoms were obvious, and a Rose Bengal test was positive. A lip biopsy specimen showed periacinar lymphocytic infiltration. Second sural nerve biopsy on the other side showed severe large fibre loss as well as small fibre loss without axonal sprouts.

DISCUSSION

The most well recognised form of Sjögren's syndrome associated neuropathy has been sensory ataxic neuropathy associated with profound impairment of kinesthetic sensation.[1-4 8-10] Neuropathologically, T cell invasion in the dorsal root ganglion as well as loss of large ganglion neurons and their large axons have been verified.[4] However clinicopathological findings in our patients differed remarkably from those of sensory ataxic neuropathy. Painful sensation and hyperalgia in our patients suggested involvement of small nociceptive nerve fibres as has been demonstrated.[11]

Indeed, in sural nerve of our patients, small myelinated and unmyelinated fibres were predominantly involved; electrophysiologically, amplitudes of SNAPs were comparatively preserved, particularly in contrast with sensory ataxic neuropathy. Findings in the dorsal root ganglion in this neuropathy have not been described, but predominant small fibre loss, extremely rare axonal sprouts, lack of vasculitis, lack of motor involvement, and fairly well preserved SEPs suggest that small dorsal root ganglion neurons can be involved.

As demonstrated by the clinical course of our patients, some patients show persistent symptoms or a slowly progressive course while remaining limited to a painful small fibre type of neuropathy, while others, including one of our patients, may later develop sensory ataxic neuropathy presumably involving large sensory neurons. Additionally, one of our patients developed localised unilateral sensory ataxia in the fingers, suggesting that some patients may develop localised sensory ataxia. These observations suggest that painful sensory neuropathy with predominant small fibre loss and sensory ataxic large fibre neuropathy are elements of a spectrum of sensory neuropathy in Sjögren's syndrome.

In summary, these patients suggest that painful sensory neuropathy with predominant small fibre loss is an identifiable subtype of Sjögren's syndrome associated neuropathy.

Authors' affiliations
K Mori, M Iijima, M Sugiura, H Koike, N Hattori, H Ito, M Hirayama, G Sobue, Department of Neurology, Nagoya University Graduate School of Medicine, Nagoya, Japan

Competing interests: none declared.

Correspondence to: Dr G Sobue, Department of Neurology, Nagoya University Graduate School of Medicine, Nagoya 466–8550 Japan; sobueg@med.nagoya-u.ac.jp

Received 31 October 2002
In revised form 26 January 2003
Accepted 14 March 2003

REFERENCES

1 **Kennett RP**, Harding AE. Peripheral neuropathy associated with the sicca syndrome. *J Neurol Neurosurg Psychiatry* 1986;**49**:90–2
2 **Graus F**, Pou A, Kanterewicz E, *et al*. Sensory neuronopathy and Sjögren's syndrome: clinical and immunologic study of two patients. *Neurology* 1988;**38**:1637–9.
3 **Gemignani F**, Marbini A, Pavesi G, *et al*. Peripheral neuropathy associated with primary Sjögren's syndrome. *J Neurol Neurosurg Psychiatry* 1994;**57**:983–6.
4 **Griffin JW**, Cornblath DR, Alexander E, *et al*. Ataxic sensory neuropathy and dorsal root ganglionitis associated with Sjögren's syndrome. *Ann Neurol* 1990;**27**:304–15.
5 **Grant IA**, Hunder GG, Homburger HA, *et al*. Peripheral neuropathy associated with sicca complex. *Neurology* 1997;**48**:855–62.
6 **Denislic M**, Meh D, Popovic M, *et al*. Small nerve fibre dysfunction in a patient with Sjögren's syndrome. Neurophysiological and morphological confirmation. *Scand J Rheumatol* 1995;**24**:257–9.
7 **Vitali C**, Bombardieri S, Jonsson R, *et al*. Classification criteria for Sjögren's syndrome: a revised version of the European criteria proposed by the American-European Consensus Group. *Ann Rheum Dis* 2002;**61**:554–8.
8 **Sobue G**, Yasuda T, Kachi T, *et al*. Chronic progressive sensory ataxic neuropathy: clinicopathological features of idiopathic and Sjögren's syndrome-associated cases. *J Neurol* 1993;**240**:1–7.
9 **Kumazawa K**, Sobue G, Yamamoto K, *et al*. Segmental anhidrosis in the spinal dermatomes in Sjögren's syndrome-associated neuropathy. *Neurology* 1993;**43**:1820–3.
10 **Mori K**, Koike H, Misu K, *et al*. Spinal cord magnetic resonance imaging demonstrates sensory neuronal involvement and clinical severity in neuronopathy associated with Sjögren's syndrome. *J Neurol Neurosurg Psychiatry* 2001;**71**:488–92.
11 **Wokke JH**, van Dijk GW. Sensory neuropathies including painful and toxic neuropathies. *J Neurol* 1997;**244**:209–21.

Cytogenet Genome Res 100:243–251 (2003)
DOI: 10.1159/000072860

Cytogenetic and Genome Research

Transgenic mouse models of spinal and bulbar muscular atrophy (SBMA)

M. Katsuno, H. Adachi, A. Inukai and G. Sobue

Department of Neurology, Nagoya University Graduate School of Medicine, Nagoya (Japan)

Abstract. Spinal and bulbar muscular atrophy (SBMA) is a late-onset motor neuron disease characterized by proximal muscle atrophy, weakness, contraction fasciculations, and bulbar involvement. Only males develop symptoms, while female carriers usually are asymptomatic. A specific treatment for SBMA has not been established. The molecular basis of SBMA is the expansion of a trinucleotide CAG repeat, which encodes the polyglutamine (polyQ) tract, in the first exon of the androgen receptor (AR) gene. The pathologic hallmark is nuclear inclusions (NIs) containing the mutant and truncated AR with expanded polyQ in the residual motor neurons in the brainstem and spinal cord as well as in some other visceral organs. Several transgenic (Tg) mouse models have been created for studying the pathogenesis of SBMA. The Tg mouse model carrying pure 239 CAGs under human AR promoter and another model carrying truncated AR with expanded CAGs show motor impairment and nuclear NIs in spinal motor neurons. Interestingly, Tg mice carrying full-length human AR with expanded polyQ demonstrate progressive motor impairment and neurogenic pathology as well as sexual difference of phenotypes. These models recapitulate the phenotypic expression observed in SBMA. The ligand-dependent nuclear localization of the mutant AR is found to be involved in the disease mechanism, and hormonal therapy is suggested to be a therapeutic approach applicable to SBMA.

Numerous animal models of neurodegenerative diseases have been created to elucidate the molecular pathogenesis and develop therapeutic approaches. Some transgenic mouse models of SBMA, the first polyglutamine (polyQ) disease to be discovered, recapitulate the symptoms and pathologic features of the disease, and provide insight into its pathogenesis. Moreover, with our latest model, we developed an effective treatment for SBMA. Here we review transgenic mouse models of SBMA, and discuss the therapeutic strategies against SBMA as well as other polyQ diseases.

Supported by a Center-of-Excellence (COE) grant from the Ministry of Education, Culture, Sports, Science and Technology, Japan, and grants from the Ministry of Health, Labor and Welfare, Japan.

Received 30 September 2002; accepted 30 January 2003.

Request reprints from Gen Sobue, MD, PhD, Department of Neurology Nagoya University Graduate School of Medicine, 65 Tsurumai-cho Showa-ku, Nagoya, 466-8550 (Japan); telephone: +81-52-744-2385 fax: +81-52-744-2384; e-mail: sobueg@med.nagoya-u.ac.jp

Spinal and bulbar muscular atrophy (SBMA)

SBMA, also known as Kennedy's disease, is a late-onset motor neuron disease characterized by proximal muscle atrophy, weakness, contraction fasciculations, and bulbar involvement (Kennedy et al., 1968; Sobue et al., 1989). Lower motor neurons are markedly depleted through all spinal segments and in brainstem motor nuclei except for the third, fourth and sixth cranial nerves (Sobue et al., 1989). Sensory neurons in the dorsal root ganglia are less severely affected, and there is also a distally accentuated sensory axonopathy in the peripheral nervous system. This disease affects males, and male patients often show signs of androgen insensitivity such as gynecomastia, testicular atrophy, and decreased fertility (Fig. 1). Female carriers are usually asymptomatic, although some express subclinical phenotypes, including high amplitude motor unit potentials on electromyography (Sobue et al., 1993; Mariotti et al., 2000; Schmidt et al., 2002). No specific treatment for SBMA has been established. Testosterone may improve motor function in some patients, although it has no effect on the progression of SBMA (Danek et al., 1994; Goldenberg et al., 1996; Neuschmid-Kaspar et al., 1996).

KARGER

Fax + 41 61 306 12 34
E-mail karger@karger.ch
www.karger.com

0301–0171/03/1004–0243$19.50/0

Accessible online at:
www.karger.com/cgr

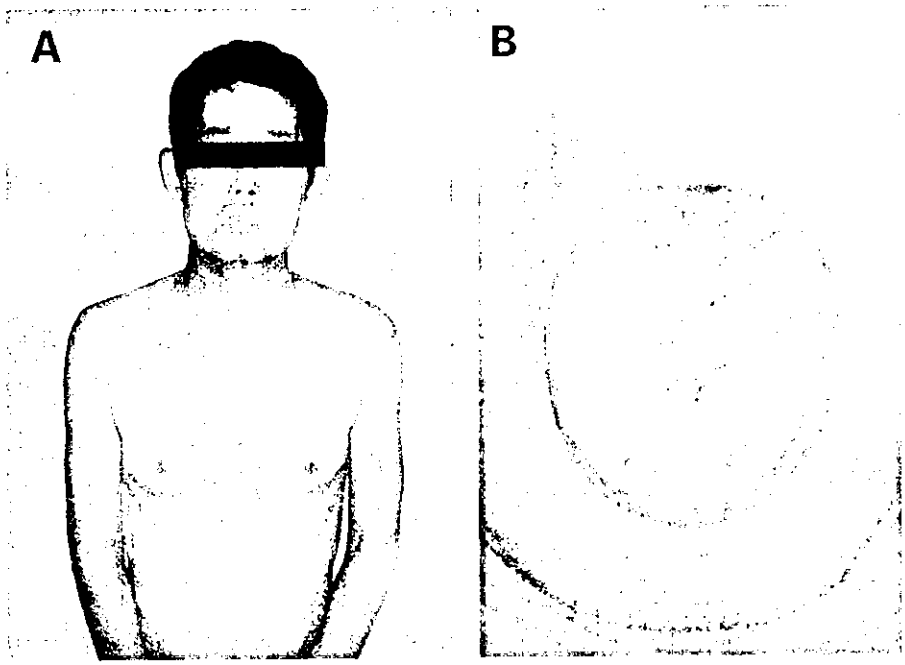

Fig. 1. SBMA patient. SBMA patients show muscle atrophy of the upper arms and gynecomastia (**A**) as well as tongue atrophy (**B**).

The molecular basis of SBMA is the expansion of a trinucleotide CAG repeat, which encodes the polyQ tract, in the first exon of the androgen receptor (AR) gene (La Spada et al., 1991). The CAG repeat within AR ranges in size from 5 to 33 repeats in normal subjects, but from 40 to 62 in SBMA patients (Tanaka et al., 1996, Merry, 2001). Expanded polyQ tracts have been found to cause several neurodegenerative diseases, including SBMA, Huntington's disease (HD), several forms of spinocerebellar ataxia, and dentatorubral and pallidoluysian atrophy (DRPLA) (Zoghbi and Orr, 2000). These disorders, known as polyQ diseases, share salient clinical features such as anticipation, somatic mosaicism (Tanaka et al., 1999), and selective neuronal and non-neuronal involvement despite widespread expression of the mutant gene (Doyu et al., 1994). There is also an inverse correlation between the CAG repeat size and the age at onset, or the disease severity adjusted by the age at examination in SBMA (Doyu et al., 1992; La Spada et al., 1992) as well as other polyQ diseases (Zoghbi and Orr, 2000).

Previously we reported nuclear inclusions (NIs) containing the mutant and truncated AR with expanded polyQ in the residual motor neurons in the brain stem and spinal cord (Li et al., 1998a) as well as in the skin, testis and some other visceral organs of SBMA patients (Li et al., 1998b). These inclusions had similar epitope features detectable by antibodies that recognize a small portion of the N-terminus of the AR protein only, and they were ubiquitinated. The presence of NIs is a pathologic hallmark of most other polyQ diseases, and is likely to be related to pathogenesis (Zoghbi and Orr, 2000). Although considerable controversy surrounds the importance of NIs in the pathogenesis of the polyQ diseases (Tobin and Signer, 2000), several studies have implied that nuclear localization of mutant protein is essential for inducing neuronal cell dysfunction and degeneration in the majority of polyQ diseases (Ross 2002). Although molecular mechanisms still remain to be elucidated, several studies have revealed that nuclear accumulation of the mutant protein resulted in sequestration of transcriptional regulatory proteins in polyQ diseases (Steffan et al., 2000; Nucifora et al., 2001).

SBMA is unique among polyQ diseases in that the mutant protein, AR, has a specific ligand, testosterone, which alters the subcellular localization of the protein by favoring its nuclear uptake. No ligands of causative protein have been found in other polyQ diseases. AR is normally confined to a multi-heteromeric inactive complex in the cell cytoplasm, and translocates into the nucleus in a ligand-dependent manner (Zhou et al., 1994; Zhou et al., 1995). This intracellular trafficking of AR may play an important role in the pathogenesis of SBMA.

Early mouse models of SBMA failed to show phenotypes

All of the available animal models of SBMA are transgenic mice with truncated or full-length human AR (Table 1). Transgenic mice were first created using the full-length AR containing 45 CAGs, which is equivalent to the repeat length observed in SBMA patients, driven by the interferon-inducible Mx promoter or the neuron-specific enolase (NSE) promoter (Bingham et al., 1995). Expression of mutant AR was found in mice with the inducible Mx promoter, but at a lower level than normal endogenous expression. The mice demonstrated neither phenotype nor repeat length instability.

Another transgenic mouse model was created with yeast artificial chromosomes (YACs) carrying the AR gene in the context of flanking non-coding sequences (La Spada et al., 1998). Studies on independent lines of AR YAC transgenic mice carrying 45 CAGs revealed intergenerational instability, which was greater with maternal transmission and with age of the transmitting mother. However, this model failed to show

Table 1. Comparison between transgenic mouse lines and SBMA patients

Reference	Transgene construct	CAG repeat instability	Motor impairment		Neuropathology		Muscle pathology
			Symptoms	Gender effect	Nuclear inclusions	Cell loss	
Bingham et al., 1995	Mx or NSE promoter, full-length human AR with 45 CAGs	(-)	(-)	(-)	(-)	(-)	(-)
LaSpada et al., 1998	YAC transgenic full-length human AR, with 45 CAGs	mild	(-)	(-)	(-)	(-)	(-)
Merry et al., 1996	NSE or NFL promoter, full-length human AR with 66 CAGs	(-)	(-)	(-)	(-)	(-)	(-)
Adachi et al., 2001	human AR promoter, sole 239 CAGs	mild	weakness, amyotrophy, incoordination	(-)	spinal cord, cerebrum cerebellum	(-)	(-)
Abel et al., 2001	NFL promoter, truncated human AR with 112 CAGs	(-)	weakness, foot clasping	(-)	spinal cord, cerebrum brainstem	(-)	(-)
Abel et al., 2001	PrP promoter, truncated human AR with 112 CAGs	(-)	hypoactivity, foot clasping, tremor, seizure	(-)	all neurons	(-)	(-)
Katsuno et al., 2002	chicken ß-actin promoter, full-length human AR with 97 CAGs	(-)	weakness, amyotrophy	significant	spinal cord, cerebrum brainstem	(-)	grouped atrophy
McManamny et al., 2002	cytomegalovirus promoter, full-length human AR with 120 CAGs	(-)	weakness, amyotrophy, foot clasping	mild	(-)	(+)	grouped atrophy fiber-type grouping hypertrophic fiber
Kennedy et al., 1968 Sobue et al., 1989	SBMA patients	mild	weakness, amyotrophy, fasciculation	significant	spinal cord, brainstem	(+)	grouped atrophy fiber-type grouping hypertrophic fiber

the expression of mutant AR in RT-PCR or Western blot analysis.

In order to enhance the toxicity of mutant AR, a transgenic mouse model was created with human AR containing 66 CAGs, which was longer than the longest repeat observed in SBMA patients, driven by the NSE promoter or the neurofilament light chain (NFL) promoter (Merry et al., 1996). Although expression levels of mutant AR were 2–5 times the endogenous AR levels, these mice showed no neurologic symptoms, presumably because the CAG repeat was not long enough.

Transgenic mouse models with truncated AR recapitulate neurologic symptoms

Since mouse models of SBMA could not be created using full-length AR, truncated AR with an expanded CAG repeat was used in later models. This strategy was based on the results reported on transgenic mice of Huntington disease and Machado-Joseph disease, where truncated protein had a particularly pronounced effect (Ikeda et al., 1996; Mangiarini et al., 1996). In SBMA and other polyQ diseases, NIs are detected by antibodies against an N-terminal epitope, but not by antibodies against a C-terminal epitope (Li et al., 1998a, b; DiFiglia et al., 1997). These findings suggest that truncated polyQ-containing proteins confer the toxicity in polyQ diseases. It should be noted that truncated mutant AR is more toxic than the full-length AR in an SBMA cell model (Merry et al., 1998; Kobayashi et al., 2000). Additionally, in vitro translated full-length AR protein with an expanded polyQ tract is cleaved by caspase-3, liberating a polyQ-containing fragment, and the susceptibility to cleavage is polyQ repeat length-dependent (Kobayashi et al., 1998). Thus, cleavage of polyQ-containing proteins is likely to contribute the toxicity of polyQ tracts.

Not like previous models, a transgenic mouse model carrying 239 CAGs driven by the human AR promoter demonstrated motor impairment and revealed that the polyQ tract is sufficient to induce the pathogenic process of SBMA (Adachi et al., 2001). Symptomatic lines exhibited small body size, weakness, truncal and limb incoordination, reduced activity and short lifespan. These phenotypes apparently developed within 4–8 weeks of birth in both lines, and gradually became severe at 8–16 weeks. Impairment of the rotarod task appeared within 8 weeks of birth, and the subsequent progression was monophasic. The most striking pathologic observation was widespread occurrence of NIs, which were distributed in the neuronal cell nuclei in the cerebrum, cerebellum, brainstem and spinal cord, but to a lesser extent or not at all in the basal ganglia. This pathologic distribution was limited by the promoter used, and was more widely spread than that of human SBMA. In the regions with their marked occurrence, the NIs were also prominently observed in the nuclei of the glial cells. The electron microscopic structure of NIs was very similar to that observed in SBMA patients; granular materials densely aggregate without a limiting membrane or filamentous materials. These NIs were positive for ubiquitin and colocalized with proteasome components (20s, PA28α, and PA28γ). Despite abundant NIs, there was no evidence of active neuronal degeneration or reactive astrogliosis. Thus neuronal dysfunction, rather than neuronal degeneration, is likely to be the pathogenesis of this mouse model. Expression of the transgene assessed by RT-PCR was revealed in the cerebrum, cerebellum, spinal cord, pituitary, lung, eye and skin; its distribution was compatible to that of NIs as well as mouse AR distribution. The mice showed subtle meiotic instability of the CAG repeat, in agreement with SBMA.

Simultaneously, another SBMA mouse model was created with truncated human AR containing 112 CAGs, driven by the

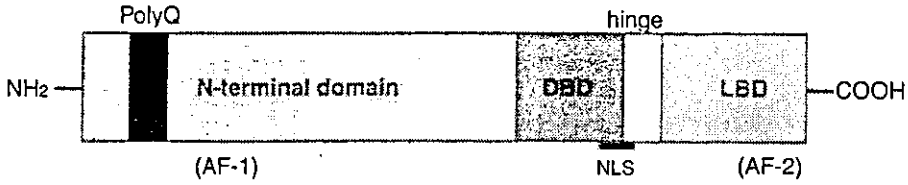

Fig. 2. Structure of AR protein. The AR protein consists of three major domains: N-terminal transactivating, DNA-binding, and ligand-binding domains. The polyglutamine tract is located in an N-terminal domain, which possesses major transactivating function (AF-1). The ligand binding domain (LBD) in the C-terminus also contains weak transactivating function (AF-2). The nuclear localization signal (NLS) in the DNA-binding domain (DBD) and hinge lesion is unmasked upon ligand-binding.

NFL or prion protein promoter (Abel et al., 2001). The mice with the prion protein promoter showed non-specific features such as tremor, seizure and loss of body weight, whereas those with the NFL promoter demonstrated motor impairment similar to SBMA patients, accompanied by upper motor deficits. Widely expressed mutant AR may account for these neurological phenotypes, because the distribution of histopathological involvement, which depended on the expression level of the transgene, was more extensive than that of SBMA. Immunohistochemical analysis of AR expression revealed transgenic AR-positive nuclear inclusions in isolated neurons in several restricted regions of the central nervous system including the brainstem and the cortex and at lower frequency in spinal cord motor neurons. NIs were ubiquitinated and contained several molecular chaperones, including HDJ-2 and Hsc70. About half of the NIs were positive for CREB-binding protein, a transcriptional coactivator (McCampbell et al., 2000). In spite of neurologic symptoms and NIs, neither neuronal loss nor neurogenic muscle atrophy was demonstrated in this model.

The fact that neuronal loss is not evident despite abundant NIs has been demonstrated in various mouse models of other polyQ diseases (Rubinsztein, 2002). Formation of NIs preceded cerebellar ataxia in a transgenic mouse model of SCA1 (Burright et al., 1995). Loss of cerebellar Purkinje cells, however, was not revealed until the symptoms progressed in this model. The life span of these model mice may not be long enough to demonstrate neuronal cell loss, although some other models have shown neuronal degeneration (Reddy et al., 1998; Hodgson et al., 1999; McManamny et al., 2002). These findings suggest that the pathogenesis of human polyQ disease could be neuronal dysfunction rather than neuronal loss in early stages.

Symptomatic full-length model provides therapeutic approach to SBMA

Unlike the profound gender difference of phenotypes in SBMA patients, neither a Tg mouse model of SBMA expressing expanded pure 239 CAGs (Adachi et al., 2001) nor another model carrying truncated AR with 112 CAGs (Abel et al., 2001) showed any remarkable phenotypic difference with gender, because the transgenes of these Tg mice did not contain the ligand-binding domain located in the C-terminus of AR (Fig. 2).

Recently, we generated Tg mice expressing the full-length human AR containing 24 or 97 CAGs under the control of the cytomegalovirus enhancer and the chicken β-actin promoter (Katsuno et al., 2002). This model recapitulated not only the neurologic disorder, but also the phenotypic difference with gender which is a specific feature of SBMA. Three out of five lines with 97 CAGs (AR-97Q) exhibited progressive motor impairment, although no lines with 24 CAGs showed any manifested phenotypes. All symptomatic lines showed small body size, muscle atrophy, weakness, reduced activity and short lifespan; all of which were markedly pronounced and accelerated in the male AR-97Q mice, but either not observed or far less severe in the female AR-97Q mice regardless of the line. Early mortality of male mice, which is not common in SBMA, appears to be caused by cachexia due to progressive amyotrophy. Western blot analysis revealed the transgenic protein retained in the stacking gel in all symptomatic lines. We detected these proteins in the spinal cord, cerebrum, heart, muscle and pancreas. Although the male AR-97Q mice had more protein within the stacking gel than their female counterparts, the female AR-97Q mice had more monomeric AR protein. The nuclear fraction contained most of the mutant AR within the stacking gel. Despite the profound sexual difference of the mutant AR protein expression, there was no significant difference in the expression of the transgene mRNA between the male and female AR-97Q mice. These observations indicate that the testosterone level plays important roles in the sexual difference of phenotypes, especially in the post-transcriptional stage of the mutant AR.

In the AR-97Q mice, we detected diffuse nuclear staining and less frequent NIs with 1C2, an antibody specifically recognizing the expanded polyQ, in the neurons of the spinal cord, cerebrum, cerebellum, brainstem and dorsal root ganglia as well as non-neuronal tissue such as the heart, muscle and pancreas. The regions with diffuse nuclear staining and NIs also showed immunoreactivity to an antibody to AR (N-20). Neither 1C2 nor N-20 revealed immunoreactivity in the cytoplasm. The male AR-97Q mice showed markedly more abundant diffuse nuclear staining and NIs than females, in agreement with the symptomatic and Western blot profile differences with gender. Muscle histology revealed significant grouped atrophy and small angulated fibers in the male AR-97Q mice as well as mild myopathic change. Although neuronal cell loss was not evident in the spinal cord, morphologic studies

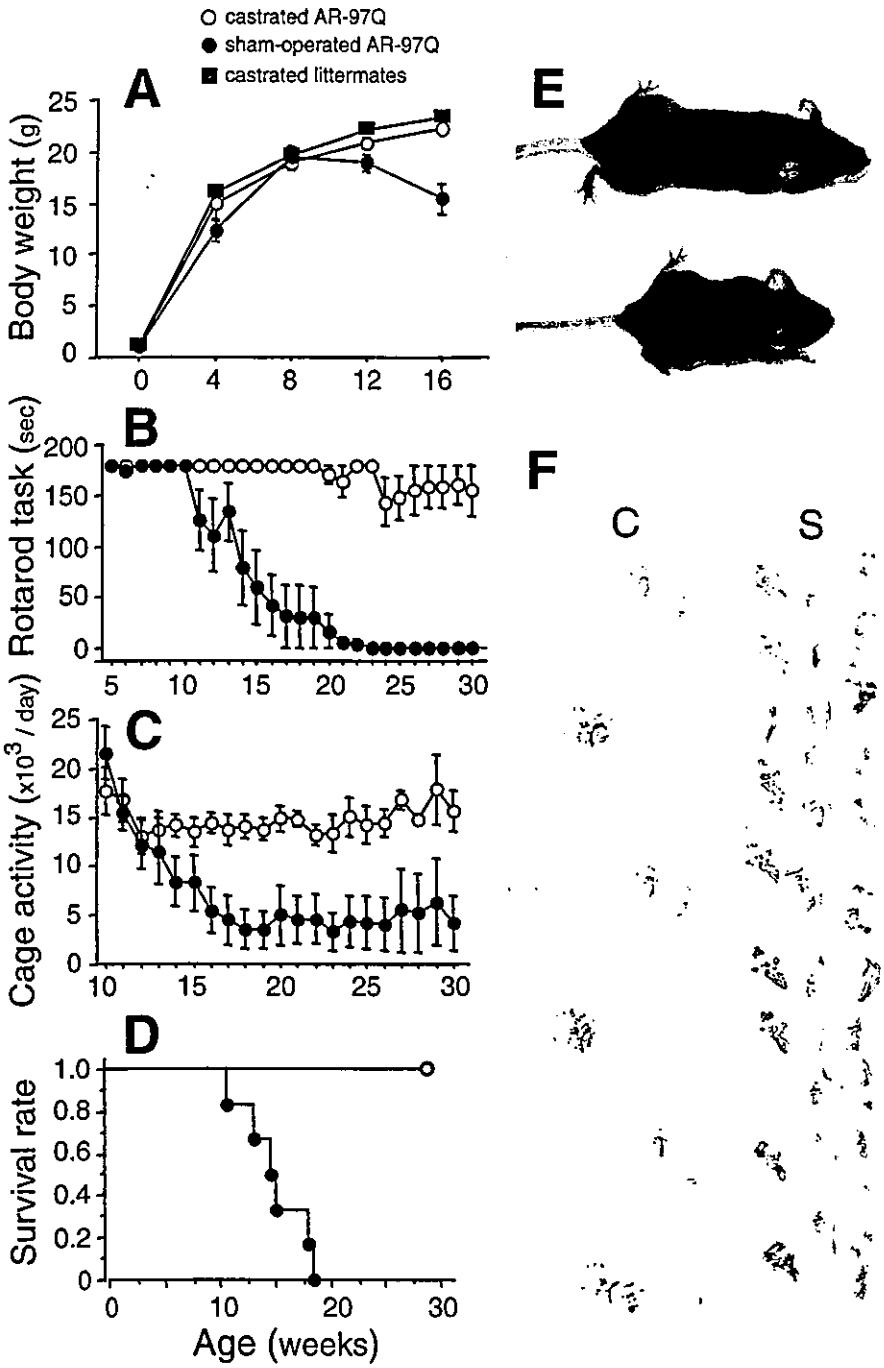

Fig. 3. Effects of castration on symptomatic phenotypes of male AR-97Q mice. (**A**, **B**, **C** and **D**). Body weight (**A**), rotarod task (**B**), cage activity (**C**), and survival rate (**D**) of castrated (○, $n = 6$) and sham-operated (●, $n = 6$) male AR-97Q mice. All parameters are significantly different between sham-operated male AR-97Q mice and castrated male AR-97Q mice or castrated male littermates (■, $n = 2$) ($P = 0.0001$, $P < 0.0001$, $P = 0.006$, and $P = 0.0006$, respectively). (**E**) A castrated AR-97Q mouse (top) shows no muscular atrophy, which is striking in a sham-operated male AR-97Q mouse (bottom) (#2-6, 12-week-old). (**F**) Footprints of 12-week-old castrated (C) and sham-operated (S) male AR-97Q mice. Front paws are in red, and hind paws in blue.

revealed axonal atrophy of the ventral nerve root as well as shrinkage of the spinal motor neurons. The female AR-97Q mice showed no neurogenic changes. The neuronal cell populations in the cerebrum, cerebellum and dorsal root ganglia were also fairly well preserved despite the abundant diffuse nuclear staining and NIs. These results indicate that dysfunction of the lower motor neurons contributes to the motor impairment in this model, and this dysfunction is far more severe in the male Tg mice than in the females.

Because of such dramatic sexual difference of phenotype, we examined the effects of hormonal interventions in this mouse model. Castrated male AR-97Q mice, which had a decreased testosterone level, showed significant improvement of symptoms, pathologic findings, and nuclear localization of the mutant AR compared with the sham-operated male AR-97Q mice. The castrated male AR-97Q mice weighed the same as their castrated male littermates, whereas the sham-operated male AR-97Q mice showed progressive emaciation (Fig. 3A). Motor impairment assessed by rotarod and cage activity was significantly less or virtually absent in the castrated male AR-97Q mice as compared with the sham-operated male AR-97Q mice (Fig. 3B and C). The castrated male AR-97Q mice showed

motor impairment similar to that of the female AR-97Q mice. The life span was also significantly prolonged in the castrated male AR-97Q mice (Fig. 3D). Castration ameliorated muscle atrophy and body size reduction (Fig. 3E). In a foot print analysis, the sham-operated male AR-97Q mice exhibited motor weakness with dragging of their legs, while the castrated male AR-97Q mice had mild symptoms (Fig. 3F). In the Western blot analysis using N-20, the mutant AR appearing within the stacking gel was markedly diminished in the castrated male AR-97Q mice compared with the sham-operated male AR-97Q mice (Fig. 4A). The mutant AR in the nuclear fraction also significantly decreased in the castrated male AR-97Q mice (Fig. 4B). Castration markedly diminished diffuse nuclear staining and NIs (Fig. 4C). These observations suggested that castration markedly prevented nuclear localization of the mutant AR protein. Leuprorelin, an LHRH agonist that reduces testosterone release from the testis, also rescued motor dysfunction and nuclear accumulation of mutant AR in this model (Katsuno et al., 2003).

In contrast to castration of the male mice, testosterone administered to the female AR-97Q mice caused significant exacerbation of symptoms, pathologic features, and nuclear localization of the mutant AR. The motor impairment assessed by rotarod and cage activity was significantly exacerbated in the female AR-97Q mice administered testosterone, similar to the case of untreated male AR-97Q mice. Western blot analysis using N-20 revealed the mutant AR in the stacking gel in whole tissue homogenates as well as in the nuclear fraction, which was larger in amount in the testosterone-administered female AR-97Q mice than in the sesame oil-administered female AR-97Q mice. The testosterone-administered female AR-97Q mice demonstrated markedly pronounced diffuse nuclear staining and NIs with 1C2 compared with the sesame oil-administered female AR-97Q mice. Since the nuclear translocation of AR is testosterone-dependent (Stenoien et al., 1999; Simeoni et al., 2000), testosterone appears to show toxic effects in the female AR-97Q mice by accelerating nuclear translocation of the mutant AR. By contrast, castration prevented the nuclear localization of the mutant AR by reducing the testosterone level. Although a few exceptions have been reported (Hodgson et al., 1999; Hackam et al., 1999), the nuclear localization of the mutant protein with expanded polyQ is important in inducing neuronal cell dysfunction and degeneration in the majority of polyQ diseases. Addition of a nuclear export signal to the mutant huntingtin eliminated aggregate formation and cell death in cell models of HD (Saudou et al., 1998; Peters et al., 1999), whereas a nuclear localization signal had the opposite effect (Peters et al., 1999). In Tg mice of SCA1 having a mutated nuclear localization signal, ataxin-1 was distributed in the cytoplasm, and the mice did not show any neurologic disorders (Klement et al., 1998). These findings suggest that reduction of testosterone ameliolates phenotypic expression by preventing nuclear localization of the mutant AR, while castration may enhance the protective effects of heat shock proteins (HSPs), which are normally associated with AR and dissociate upon ligand binding.

The castrated AR-97Q mice showed phenotypes similar to those of the female AR-97Q mice, implying that motor impairment in SBMA patients can be reduced to the level in female carriers. SBMA has been considered to be an X-linked disease, whereas other polyQ diseases show autosomal dominant inheritance. In fact, SBMA female carriers hardly manifest clinical phenotypes, although they possess similar numbers of a CAG repeat in the disease allele as their siblings with SBMA (Sobue et al., 1993; Mariotti et al., 2000). Indeed the lower level of mutant AR expression in female carriers due to X inactivation may cause the escape from the manifestation, but our present study also strongly suggests that the low level of testosterone prevents the nuclear localization of the expressed mutant AR, resulting in a lack of phenotypic manifestations in the female carriers. This hypothesis is supported by the finding that manifestation of symptoms is minimal even in homozygous females of SBMA (Schmidt et al., 2002). The testosterone-dependent neurodegenaration was also recently revealed in a fly model of SBMA (Takeyama et al., 2002). Thus, hormonal intervention to diminish testosterone level appears to be applicable to human therapy.

Another Tg mouse model carrying the full-length AR with 120 CAGs driven by the cytomegalovirus promoter showed slowly progressive motor impairment and neurogenic muscle atrophy (McManamny et al., 2002). The affected mice also displayed a progressive reduction in sperm production consistent with androgen insensitivities in SBMA patients. Although this model showed no neuronal inclusions throughout the nervous system, loss of motor neurons was demonstrated in the spinal cord. Notably, as expected, mild but evident sexual difference of phenotypes was observed. This finding supports the hypothesis that testosterone level is implicated in the phenotypic expression of SBMA. The above study and ours indicate that the C-terminus of mutant AR is necessary to recapitulate the testosterone-dependent pathogenesis of SBMA in mouse models.

"Loss of function" model of SBMA

As in other autosomal dominant polyQ diseases, a toxic gain of the mutant AR function has been considered the mainstream of SBMA pathogenesis. Although the expansion of polyQ tract in AR deteriorates the transcriptional activities of AR (Mhatre et al., 1993; Brooks et al., 1997), motor impairment has not been observed in severe testicular feminization (Tfm) patients lacking AR function (Gottlieb et al., 1999). Thus, the neurologic impairment in SBMA cannot be attributed to the loss of AR function (Maclean et al., 1995), a reason why testosterone shows insufficient and transient effects when used as a therapeutic agent for SBMA (Danek et al., 1994; Goldenberg et al., 1996; Neuschmid-Kaspar et al., 1996). Animal models of Tfm demonstrate a decreased number of motor neurons in the spinal nucleus of the bulbocavernosus (Sengelaub et al., 1989) without any other motor neuron involvement.

However, re-examination of earlier studies and recent data has revealed that loss of normal protein function also plays a role in the neuronal involvement in polyQ diseases. In a huntingtin knockout mouse model, the heterozygotes demonstrated motor impairment and basal ganglia degeneration (Na-

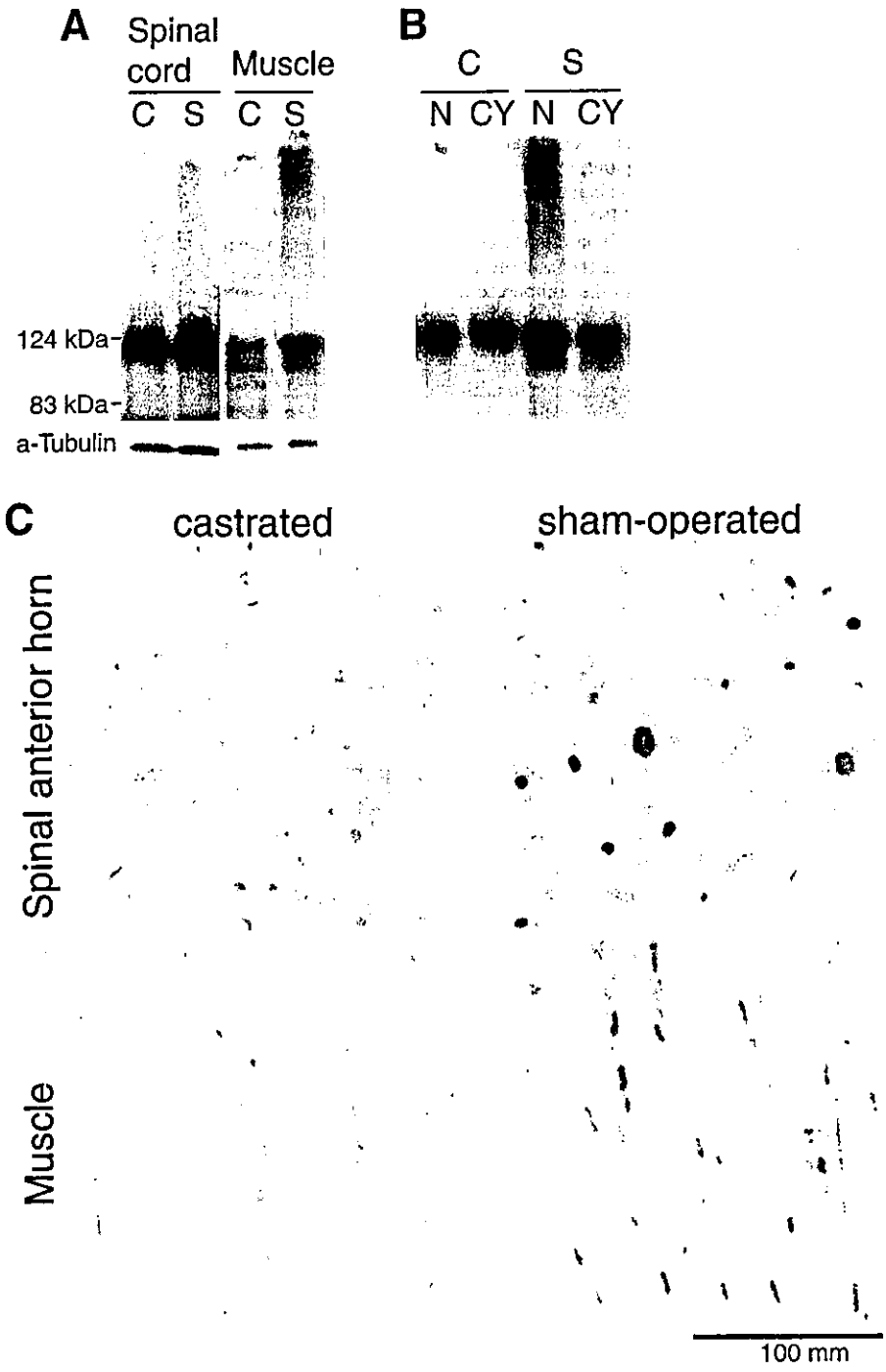

Fig. 4. Effects of castration on transgene expression and neuropathology of male AR-97Q mice. **(A)** Western blot analysis of total homogenates from the spinal cord and muscle of castrated (C) and sham-operated (S) male AR-97Q mice, that were immunolabeled by N-20. **(B)** Western blot analysis of nuclear (N) and cytoplasmic (CY) fraction from muscle of castrated (C) and sham-operated (S) male AR-97Q mice, immunolabeled by N-20. **(C)** Immunohistochemical study using 1C2 showed marked differences of diffuse nuclear staining and nuclear inclusions between castrated and sham-operated AR-97Q mice in the spinal anterior horn and muscle.

sir et al., 1995). More recently, conditional inactivation of wild-type huntingtin selectively in forebrain and testis resulted in a progressive degenerative neuronal phenotype and sterility (Dragatsis et al., 2000). Additionally, an anti-apoptotic effect of wild-type huntingtin was revealed in a cell model (Rigamonti et al., 2000). These results imply that loss of normal huntingtin function may contribute to the neurodegeneration in HD.

Androgens have been found to have neuroprotective effects. Administration of testosterone immediately after nerve injury impacts positively on functional recovery through actions mediated by the androgen receptor (Jones at al., 2001). In a cell culture model, AR with 24 CAGs showed trophic effects, whereas AR with 65 CAGs did not demonstrate any neuroprotection (Lieberman et al., 2002). The role of normal AR function in the pathogenesis of SBMA should be further studied in cell and animal models.

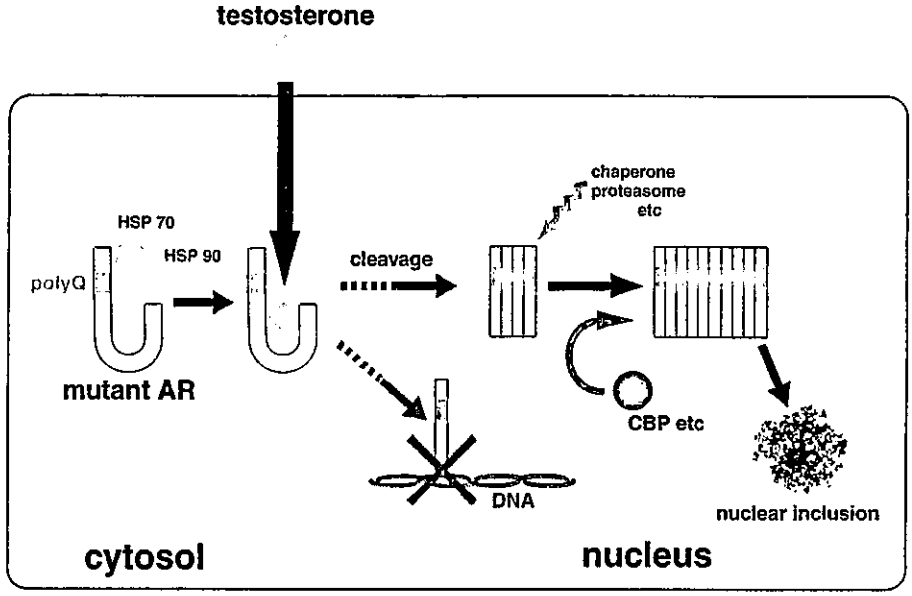

Fig. 5. Hypothetical dynamics of mutant AR in SBMA. In the absence of ligand, mutant AR is confined to a multi-heteromeric inactive complex with heat shock proteins (HSPs) and immunophilins in the cell cytoplasm. Upon testosterone-binding, the conformational change of mutant AR facilitates its dissociation from the complex and translocation into the nucleus. Mutant AR is cleaved and aggregates in the nucleus, whereas cellular mechanisms such as molecular chaperone and ubquitin-proteasome system attempt to mitigate its toxicity. Aggregation sequestrates critical cellular proteins such as CREB-binding protein (CBP) resulting in aberrant transcription, and finally forms nuclear inclusions. On the other hand, decreased transactivating function of mutant AR may contribute to the neurodegeneration and androgen insensitivity in SBMA.

Toward therapy for SBMA and other polyQ diseases

As mentioned above, our recent study indicated that testosterone reduction exerts therapeutic effects by preventing nuclear translocation of mutant AR in the SBMA transgenic mouse model (Fig. 5). This approach can easily be applied to human SBMA therapy. Although no specific ligand of the mutant protein has been revealed in other polyQ diseases, the striking therapeutic effects of castration in our SBMA mice further suggest that patients with polyQ disease can be rescued by preventing the nuclear translocation of the mutant proteins. We emphasize the need of investigating hormone-like small molecules which alter the nuclear localization of mutant proteins for developing therapeutic intervention.

No substantially effective therapeutic approach to polyQ diseases has been developed in spite of continuous efforts. However, some promising results using transgenic animal models have been reported. Molecular chaperones, which renature misfolded mutant proteins, have exerted beneficial effects in cell and animal models of polyQ diseases (Kobayashi et al., 2001). Over-expression of molecular chaperone HSP70 had preventive effects in cell and Tg mouse models of SBMA (Kobayashi et al., 2000; Adachi et al., 2003) as well as in an SCA1 Tg mouse model (Cummings et al., 2001). It may also be possible to treat SBMA by increasing the expression level or enhancing the function of molecular chaperones.

Alternatively, histone deacetylase inhibitors could be a promising candidate therapy for polyQ diseases (Steffan et al., 2001; Hockly et al., 2003). These drugs potentially correct altered transcription due to toxic effects of the mutant protein containing expanded polyQ, although their toxicity should be conquered before clinical application.

In the near future, an ideal treatment for polyQ diseases could be a combination of these and other therapeutic strategies. Transgenic mice will be useful in testing the effectiveness of therapies, and further contribute to the development of a strategy against polyQ diseases including SBMA.

Acknowledgements

Figures 3 and 4 are reprinted from Katsuno et al. (2002) with permission from Elsevier Science.

References

Abel A, et al: Expression of expanded repeat androgen receptor produces neurologic disease in transgenic mice. Hum molec Genet 10:107–116 (2001).

Adachi H, et al: Transgenic mice with an expanded CAG repeat controlled by the human AR promoter show polyglutamine nuclear inclusions and neuronal dysfunction without neuronal cell death. Hum molec Genet 10:1039–1048 (2001).

Adachi H, et al: HSP70 chaperone over-expression ameliorates phenotypes of the SBMA transgenic mouse model by reducing nuclear-localized mutant AR protein. J Neurosci 23:2203–2211 (2003).

Bingham PM, et al: Stability of an expanded trinucleotide repeat in the androgen receptor gene in transgenic mice. Nature Genet 9:191–196 (1995).

Brooks BP, et al: Characterization of an expanded glutamine repeat androgen receptor in a neuronal cell culture system. Neurobiol Dis 3:313–323 (1997).

Burright EN, et al: SCA1 transgenic mice: a model for neurodegeneration caused by an expanded CAG trinucleotide repeat. Cell 82:937–948 (1995).

Cummings CJ, et al: Over-expression of inducible HSP70 chaperone suppresses neuropathology and improves motor function in SCA1 mice. Hum molec Genet 10:1511–1518 (2001).

Danek A, et al: Decrease in androgen binding and effect of androgen treatment in a case of X-linked bulbospinal neuronopathy. Clin Investig 72:892–897 (1994).

DiFiglia M, et al: Aggregation of huntingtin in neuronal intranuclear inclusions and dystrophic neurites in brain. Science 277:1990–1993 (1997).

Doyu M, et al: Severity of X-linked recessive bulbospinal neuronopathy correlates with size of the tandem CAG repeat in androgen receptor gene. Ann Neurol 32:707–10 (1992).

Doyu M, et al: Androgen receptor mRNA with increased size of tandem CAG repeat is widely expressed in the neural and nonneural tissues of X-linked recessive bulbospinal neuronopathy. J Neurol Sci 127:43–47 (1994).

Dragatsis I, et al: Inactivation of Hdh in the brain and testis results in progressive neurodegeneration and sterility in mice. Nature Genet 26:300–306 (2000).

Goldenberg JN, et al: Testosterone therapy and the pathogenesis of Kennedy's disease (X-linked bulbospinal muscular atrophy). J Neurol Sci 135:158–161 (1996).
Gottlieb B, et al: Androgen insensitivity. Am J med Genet 89:210–217 (1999).
Hackam AS, Singaraja R, Zhang T, Gan L, Hayden MR: In vitro evidence for both the nucleus and cytoplasm as subcellular sites of pathogenesis in Huntington's disease. Hum molec Genet. 8:25–33 (1999).
Hockly E, et al: Suberoylanilide hydroxamic acid, a histone deacylase inhibitor, ameliorates motor deficits in a mouse model of Huntington's disease. Proc natl Acad Sci, USA 100:2041–2046 (2003).
Hodgson JG, et al: A YAC mouse model for Huntington's disease with full-length mutant huntingtin, cytoplasmic toxicity, and selective striatal neurodegeneration. Neuron 23:181–192 (1999).
Ikeda H, et al: Expanded polyglutamine in the Machado-Joseph disease protein induces cell death in vitro and in vivo. Nature Genet 13:196–202 (1996).
Jones KJ, et al: Neuroprotective effects of gonadal steroids on regenerating peripheral motoneurons. Brain Res Brain Res Rev 37:372–382 (2001).
Katsuno M, et al: Testosterone reduction prevents phenotypic expression in a transgenic mouse model of spinal and bulbar muscular atrophy. Neuron 35:843–854 (2002).
Katsuno M, et al: Leuprorelin rescues polyglutamine-dependent phenotypes in a transgenic mouse model of spinal and bulbar muscular atrophy. Nature Med 9:768–773 (2003).
Kennedy WR, et al: Progressive proximal spinal and bulbar muscular atrophy of late onset. A sex-linked recessive trait. Neurology 18:671–680 (1968).
Klement IA, et al: Ataxin-1 nuclear localization and aggregation: role in polyglutamine-induced disease in SCA1 transgenic mice. Cell 95:41–53 (1998).
Kobayashi Y, et al: Caspase-3 cleaves the expanded androgen receptor protein of spinal and bulbar muscular atrophy in a polyglutamine repeat length-dependent manner. Biochem biophys Res Commun 252:145–150 (1998).
Kobayashi Y, et al: Chaperones Hsp70 and Hsp40 suppress aggregate formation and apoptosis in cultured neuronal cells expressing truncated androgen receptor protein with expanded polyglutamine tract. J biol Chem 275:8772–8778 (2000).
Kobayashi Y, Sobue G: Protective effect of chaperones on polyglutamine diseases. Brain Res Bull 56:165–168 (2001).
La Spada AR, et al: Androgen receptor gene mutations in X-linked spinal and bulbar muscular atrophy. Nature 352:77–79 (1991).
La Spada AR, et al: Meiotic stability and genotype-phenotype correlation of the trinucleotide repeat in X-linked spinal and bulbar muscular atrophy. Nature Genet 2:301–304 (1992).
La Spada AR, et al: Androgen receptor YAC transgenic mice carrying CAG 45 alleles show trinucleotide repeat instability. Hum molec Genet 7:959–967 (1998).
Li M, et al: Nuclear inclusions of the androgen receptor protein in spinal and bulbar muscular atrophy. Ann Neurol 44:249–254 (1998).
Li M, et al: Nonneural nuclear inclusions of androgen receptor protein in spinal and bulbar muscular atrophy. Am J Pathol 153:695–701 (1998).
Lieberman AP, et al: Altered transcriptional regulation in cells expressing the expanded polyglutamine androgen receptor. Hum molec Genet 11:1967–1976 (2002).
MacLean HE, et al: Defects of androgen receptor function: from sex reversal to motor neuron disease. Mol Cell Endocr 112:133–141 (1995).
Mangiarini L, et al: Exon 1 of the HD gene with an expanded CAG repeat is sufficient to cause a progressive neurological phenotype in transgenic mice. Cell 87:493–506 (1996).
Mariotti C, et al: Phenotypic manifestations associated with CAG-repeat expansion in the androgen receptor gene in male patients and heterozygous females: a clinical and molecular study of 30 families. Neuromuscul Disord 10:391–397 (2000).
McCampbell A, et al: CREB-binding protein sequestration by expanded polyglutamine. Hum molec Genet 9:2197–2202 (2000).
McManamny P, et al: A mouse model of spinal and bulbar muscular atrophy. Hum molec Genet 11:2103–2111 (2002).
Merry DE, et al: Toward a mouse model for spinal and bulbar muscular atrophy: effect of neuronal expression of androgen receptor in transgenic mice. (abstract) Am J hum Genet 59 (suppl):A271 (1996).
Merry DE, et al: Cleavage, aggregation and toxicity of the expanded androgen receptor in spinal and bulbar muscular atrophy. Hum molec Genet 7:693–701 (1998).
Merry DE: Molecular pathogenesis of spinal and bulbar muscular atrophy. Brain Res Bull 56:203–207 (2001).
Mhatre AN, et al: Reduced transcriptional regulatory competence of the androgen receptor in X-linked spinal and bulbar muscular atrophy. Nature Genet 5:184–188 (1993).
Nasir J, et al: Targeted disruption of the Huntington's disease gene results in embryonic lethality and behavioral and morphological changes in heterozygotes. Cell 81:811–823 (1995).
Neuschmid-Kaspar F, et al: CAG-repeat expansion in androgen receptor in Kennedy's disease is not a loss of function mutation. Mol Cell Endocrinol 117:149–156 (1996).
Nucifora FC Jr, et al: Interference by huntingtin and atrophin-1 with CBP-mediated transcription leading to cellular toxicity. Science 291:2423–2428 (2001).
Peters MF, et al: Nuclear targeting of mutant Huntingtin increases toxicity. Mol Cell Neurosci 14:121–128 (1999).
Reddy PH, et al: Behavioural abnormalities and selective neuronal loss in HD transgenic mice expressing mutated full-length HD cDNA. Nature Genet. 20:198–202 (1998).
Rigamonti D, et al: Wild-type huntingtin protects from apoptosis upstream of caspase-3. J Neurosci 20:3705–3713 (2000).
Ross CA: Polyglutamine pathogenesis: emergence of unifying mechanisms for Huntington's disease and related disorders. Neuron 35:819–822 (2002).
Rubinsztein DC: Lessons from animal models of Huntington's disease. Trends Genet 18:202–209 (2002).
Saudou F, et al: Huntingtin acts in the nucleus to induce apoptosis but death does not correlate with the formation of intranuclear inclusions. Cell 95:55–66 (1998).
Schmidt BJ, et al: Expression of X-linked bulbospinal muscular atrophy (Kennedy disease) in two homozygous women. Neurology 59:770–772 (2002).
Sengelaub DR, et al: Hormonal control of neuron number in sexually dimorphic spinal nuclei of the rat: II. Development of the spinal nucleus of the bulbocavernosus in androgen-insensitive (Tfm) rats. J Comp Neurol 280:630–636 (1989).
Simeoni S, et al: Motoneuronal cell death is not correlated with aggregate formation of androgen receptors containing an elongated polyglutamine tract. Hum molec Genet 9:133–144 (2000).
Sobue G, et al: X-linked recessive bulbospinal neuronopathy. A clinicopathological study. Brain 112:209–232 (1989).
Sobue G, et al: Subclinical phenotypic expressions in heterozygous females of X-linked recessive bulbospinal neuronopathy. J Neurol Sci 117:74–78 (1993).
Steffan JS, et al: The Huntington's disease protein interacts with p53 and CREB-binding protein and represses transcription. Proc natl Acad Sci, USA 97:6763–6768 (2000).
Steffan JS, et al: Histone deacetylase inhibitors arrest polyglutamine-dependent neurodegeneration in Drosophila. Nature 413:739–743 (2001).
Stenoien DL, et al: Polyglutamine-expanded androgen receptors form aggregates that sequester heat shock proteins, proteasome components and SRC-1, and are suppressed by the HDJ-2 chaperone. Hum molec Genet 8:731–741 (1999).
Takeyama K, et al: Androgen-dependent neurodegeneration by polyglutamine-expanded human androgen receptor in *Drosophila*. Neuron 35:855–864 (2002).
Tanaka F, et al: Founder effect in spinal and bulbar muscular atrophy (SBMA). Hum molec Genet 5:1253–1257 (1996).
Tanaka F, et al: Tissue-specific somatic mosaicism in spinal and bulbar muscular atrophy is dependent on CAG-repeat length and androgen receptor-gene expression level. Am J hum Genet 65:966–973 (1999).
Tobin AJ, Signer ER: Huntington's disease: the challenge for cell biologists. Trends Cell Biol. 10:531–536 (2000).
Zhou ZX, et al: The androgen receptor: an overview. Recent Prog Horm Res 49:249–274 (1994).
Zhou ZX, et al: Specificity of ligand- dependent androgen receptor stabilization: receptor domain interactions influence ligand dissociation and receptor stability. Mol Endocrinol 9:208–218 (1995).
Zoghbi HY, Orr HT: Glutamine repeats and neurodegeneration. A Rev Neurosci 23:217–247 (2000).

DOI: 10.1093/brain/awh020 Advanced Access publication November 7, 2003 *Brain* (2004), **127**, 203–211

Nerve excitability properties in Charcot–Marie–Tooth disease type 1A

Hiroyuki Nodera,[1] Hugh Bostock,[4] Satoshi Kuwabara,[2] Takashi Sakamoto,[1] Kotaro Asanuma,[1] Sung Jia-Ying,[2] Kazue Ogawara,[2] Naoki Hattori,[3] Masaaki Hirayama,[3] Gen Sobue[3] and Ryuji Kaji[1]

[1]*Department of Clinical Neuroscience, Graduate School of Medicine, University of Tokushima, Tokushima,* [2]*Department of Neurology, Chiba University, Chiba,* [3]*Department of Neurology, Nagoya University, Nagoya, Japan and* [4]*Sobell Department of Neurophysiology, Institute of Neurology, Queen Square, London, UK*

Correspondence to: Ryuji Kaji, MD, PhD, Department of Clinical Neuroscience, University of Tokushima, 2-50-1 Kuramotocho, Tokushima City, 770-8503 Japan
E-mail: rkaji@clin.med.tokushima-u.ac.jp

Summary

Charcot–Marie–Tooth disease type 1A (CMT1A) is commonly considered a prototype of a hereditary demyelinating polyneuropathy. Apart from the myelin involvement, there has been little information on axonal membrane properties in this condition. Taking advantage of the uniform nature of the disease process, we undertook the *in vivo* assessment of multiple axonal excitability properties at the median nerve in nine CMT1A patients with *PMP22* (peripheral myelin protein 22) gene duplication and 53 controls. The thresholds of CMT1A patients were much higher than normal, and threshold electrotonus (TE) exhibited a consistent pattern of abnormalities: early steep changes (fanning out) of both hyperpolarizing and depolarizing responses were followed by increased inward rectification to hyperpolarizing currents and unusually fast accommodation to depolarizing currents. Strength–duration time constants and the shapes of recovery cycles were normal, although refractoriness and superexcitability were reduced relative to controls. The high thresholds and early fanning out of electrotonus indicated altered cable properties, such that a greater proportion than normal of applied currents reached internodal rather than nodal axolemma. The rapid accommodation to depolarizing currents suggested activation of fast K^+ channels, which are normally sequestered from the nodal membrane. The excitability abnormalities are therefore consistent with a demyelinating pathology and exposure or spread of K^+ channels from under the myelin. It remains to be seen whether the TE abnormalities in CMT1A, which resemble previous recordings from normal immature rats, can be distinguished from those in acquired demyelinating neuropathies.

Keywords: Charcot–Marie–Tooth disease type 1A; paranode; membrane properties; threshold tracking; potassium channel

Abbreviations: CIDP = chronic inflammatory demyelinating polyneuropathy; CMAP = compound muscle action potential; CMT1A = Charcot–Marie–Tooth disease type 1A; CV = conduction velocity; DL = distal motor latency; PMP22 = peripheral myelin protein 22; SNAP = sensory nerve action potential; TE = threshold electrotonus

Introduction

Charcot–Marie–Tooth disease type 1A (CMT1A) is the most common form of hereditary motor and sensory neuropathy and its hallmark is diffuse demyelination (Dyck *et al.*, 1993; Birouk *et al.*, 1997). However, secondary axonal degeneration is common and its degree determines the patient's functional disability (Hattori *et al.*, 2003; Krajewski *et al.*, 2000; Hanemann and Gabreels-Festen, 2002). To date, the pathophysiology of the secondary axonal degeneration in CMT1 is unknown, although abnormal axon–Schwann cell interaction has been considered to play a major role (Sahenk and Mendell, 1999*a*; Kamholz *et al.*, 2000; Maier *et al.*, 2002). Intact Schwann cells are important in maintaining axonal integrity and development (Peles and Salzer, 2000; Martini, 2001; Scherer and Arroyo, 2002), so it would be reasonable to assume that in CMT1A abnormalities exist in axonal membrane properties, as well as in myelin.

Measurements of axonal excitability properties by threshold tracking have recently shed light on a variety of conditions affecting peripheral nerves (Bostock *et al.*, 1998; Burke *et al.*, 2001). The excitability properties are particularly sensitive to membrane potential, but also depend on nodal and internodal ion channels, as well as the passive

membrane properties, such a nodal width, and the extent to which the internodal axonal compartment is electrically isolated from the nodal compartment (Bostock *et al.*, 1998). Although many of these parameters are expected to be altered in demyelinating disease, several clinical studies have failed to reveal a clear-cut pattern of excitability changes related to demyelination. Thus a study of chronic inflammatory demyelinating polyneuropathy (CIDP) found raised thresholds but a shorter strength–duration time constant and no consistent changes in threshold electrotonus (Cappelen-Smith *et al.*, 2001). Studies of multifocal motor neuropathy have found evidence of membrane hyperpolarization distal to sites of conduction block (Kiernan *et al.*, 2002*b*), reduced Na^+ conductance (Priori *et al.*, 2002) and normal membrane properties proximal to sites of block (Cappelen-Smith *et al.*, 2002), but at the sites of conduction block, where demyelination has been reported (Kaji *et al.*, 1993), thresholds are very high and specific excitability changes relatable to demyelination have not been reported. A study of axonal and demyelinating forms of Guillain–Barré syndrome (Kuwabara *et al.*, 2002*a*) also failed to find any changes in nerve excitability properties at the wrist that could be directly related to the demyelination, probably because the major pathology occurred more distally in these patients. It has previously been argued that the reason why threshold electrotonus studies have failed to reveal consistent abnormalities in demyelinating neuropathies is because axons and nodes are affected non-uniformly, and fibres demyelinated at the point of stimulation will preferentially be excited at adjacent normal nodes, or other, more normal fibres will be excited in their place (Bostock *et al.*, 1998). This argument should be less applicable to CMT1A, in which it is possible to limit cases to a well-defined genetic defect [duplication of the *PMP22* (peripheral myelin protein 22) gene] and axons are affected relatively uniformly.

This study was therefore undertaken to test the hypothesis that CMT1A patients, unlike those with previously studied acquired demyelinating diseases, would exhibit a consistent pattern of abnormal excitability measures. A further aim was to test for secondary changes in axonal membrane properties, such as changes in membrane potential, which could not be related directly to altered myelination but which might be related to the secondary axonal degeneration. In the event, a consistent pattern of abnormal nerve excitability properties was found, which was consistent with demyelination, but there was little evidence of degeneration, or excitability changes that might be related to degeneration, in the sample of patients studied.

Patients and methods

Patients

Recordings were made from nine patients with genetically proven CMT1A (aged 11–75 years; mean 48.1 years; seven males and two females) from three university hospitals in Japan. All patients showed typical but variable clinical features of CMT type 1, such as diffuse areflexia/hyporeflexia, length-dependent sensory loss, distal atrophy and foot deformities. A fluorescence *in situ* hybridization-based assay identified the 1.5 Mb duplication on chromosome 17p11.2–12 containing the *PMP22* gene in all the subjects. No patient had a past history of diabetes, connective tissue disease, malignancy, electrolyte abnormality or use of neurotoxic drugs or steroids. All the patients had a clear family history of similar symptoms and signs of autosomal dominant inheritance. All the patients (and a parent for a minor) gave informed consent to participation in the study. This study was performed in accordance with the principles embodied in the Declaration of Helsinki and the protocol was approved by institutional review boards of all participating hospitals.

Conventional nerve conduction studies

Nerve conduction studies were performed with percutaneous stimulating and recording electrodes. The distal motor latency (DL), motor nerve conduction velocity (CV) and compound muscle action potentials (CMAP) were elicited with distal and proximal stimulation from the median (in the wrist with 7 cm stimulating–recording distance, and in the elbow), ulnar (in the wrist with 7 cm stimulating–recording distance, and in the forearm) and tibial (in the ankle with 8 cm stimulating–recording distance, and in the knee) nerves. Sensory nerve action potentials (SNAPs) were recorded antidromically from the median, ulnar and sural nerves using surface recording electrodes and stimulating–recording distances of 13, 11 and 14 cm respectively.

Nerve excitability measures

Studies were performed using a recently described protocol (Kiernan *et al.*, 2000) designed to measure multiple nerve excitability parameters rapidly.

CMAPs were recorded from thenar muscles using surface electrodes over the abductor pollicis brevis on the dominant hand side, with the active electrode at the motor point and the reference on the proximal phalanx. The EMG signal was amplified (gain 1000, bandwidth 1.6 Hz to 2 kHz) and digitized by a computer (486PC) with an A/D board (DT2812; Data Translation, Marlboro, MA, USA) using a sampling rate of 10 kHz. Stimulus waveforms generated by the computer were converted to current with a purpose-built isolated linear bipolar constant-current stimulator (maximum output ± 100 mA). The stimulus currents were applied via non-polarizable electrodes (Unique Medical, Tokyo, Japan), with the active electrode over the median nerve at the wrist and the reference electrode 10 cm proximal over muscle. Stimulation and recording were controlled by QTRAC software (©Institute of Neurology, London, with multiple excitability protocol TRONDXM).

Test current pulses of 0.2 or 1 ms were applied at 0.8 s intervals, and were combined with suprathreshold condition-

Table 1 *Results of the nerve conduction studies*

Nerve	DL (ms)	CMAP amplitude (mV)	Motor CV (m/s)	SNAP amplitude (μV)	Sensory CV (m/s)
Median	8.5 (6.9–10.2)	4.7 (1.8–8.9)	22.3 (16–39)	2.1 (0–6.8)	22.4 (18–28; n^* = 5)
Ulnar	7.4 (5.9–9.1)	3.1 (0.9–4.2)	22.2 (15–38)	0.5 (0–3.0)	23 (20–26; n = 2)
Tibial	10.3 (6.5–12.1)	1.2 (0–3.2)	18.7 (13–35)		
Sural				1.47 (0–12)	23 (16–29; n = 2)

Data are mean (range). There were nine patients (seven men, two women), with mean age 48.1 years (range 11–75 years). n^* is the number of patients in whom CV was obtainable (i.e. presence of SNAP). DL = distal latency; CMAP = compound muscle action potential; CV = conduction velocity; SNAP = sensory nerve action potential.

ing stimuli or subthreshold polarizing currents as required. The polarizing, conditioning and test current pulses were all delivered through the same electrodes. The amplitude of the CMAP was measured from baseline to negative peak. For all tracking studies, the target CMAP was set to 40% of maximum. Skin temperature was recorded using an adhesive probe over the nerve, adjacent to the stimulation electrode, to monitor temperature close to the site where axonal excitability was tested. The sequence of recordings followed that previously described (Kiernan *et al.*, 2000). Stimulus–response curves were recorded separately for test stimuli of durations 0.2 and 1 ms. The stimuli were increased in 6% steps, with two responses averaged for each step, until three averages were considered maximal. The ratio between the 0.2 and 1 ms stimuli required to evoke the same response was used to estimate the strength–duration time constant of axons of different threshold. A target response was then set at 40% of the maximum and the 1.0 ms test stimuli adjusted automatically by the computer to maintain this peak CMAP amplitude. Proportional tracking was used, whereby the change in stimulus amplitude from one trial to the next was made proportional to the 'error', or the difference between the last response and the target response (Bostock *et al.*, 1998). The slope of the stimulus–response curve was used to set the constant of proportionality and to optimize the tracking efficiency. Prolonged subthreshold currents were used to alter the potential difference across the internodal as well as the nodal axonal membrane. The changes in threshold associated with these electrotonic changes in membrane potential normally have a similar time course and are known as threshold electrotonus (TE) (Bostock *et al.*, 1998). Threshold tracking was used to record the changes in threshold induced by 100 ms polarizing currents, set to 40% (depolarizing) and –40% (hyperpolarizing) of the control threshold current. Three stimulus combinations were tested in turn: (i) test stimulus alone (to measure the control threshold current); (ii) test stimulus + depolarizing conditioning current; and (iii) test stimulus + hyperpolarizing conditioning current. Threshold was tested at 26 time points (maximum separation 10 ms) before, during and after the 100 ms conditioning currents. Each stimulus combination was repeated until three valid threshold estimates were recorded, as judged by the response being within 15% of the target response or alternate responses being either side of the target. We checked for the lack of CMAP response in all the raw traces after applying only conditioning stimulation.

The current–threshold relationship was tested with 1 ms pulses at the end of 200 ms polarizing currents, which were altered in 10% steps from +50% (depolarizing) to –100% (hyperpolarizing) of the control threshold. As with the conventional TE protocol, stimuli with conditioning currents were alternated with test stimuli alone, and each stimulus combination was repeated until three valid threshold estimates had been obtained.

The final part of the protocol recorded the recovery of excitability following a supramaximal conditioning stimulus. These changes were recorded at 18 conditioning ($1/n$) test intervals, decreasing from 200 to 2 ms in approximately geometrical progression. Three stimulus combinations were tested in turn: (i) unconditioned test stimulus (of 1 ms duration) tracking the control threshold; (ii) supramaximal conditioning stimulus (1 ms duration) alone; and (iii) conditioning + test stimuli. The response to (ii) was subtracted on-line from the response to (iii) before the test CMAP was measured, so that the conditioning maximal CMAP did not contaminate the measured response when the conditioning–test interval was short. Each stimulus combination was repeated until four valid threshold estimates had been obtained.

Control data

For threshold tracking studies, control data were obtained from 53 healthy individuals with mean age 43.1 years (range 23–84 years) at Chiba University Hospital. Given the fact that additional control data from an 8-year-old girl (not included for analysis at the parent's request) has shown a similar trend of the nerve excitability properties to the adult controls, data from an 11-year-old CMT1A patient was included for the study. All subjects (and a parent for a minor) gave informed consent.

Data analysis

Values for the excitability measures obtained in the present study were compared with normative data. The Mann–Whitney *U* test or repeated measures ANOVA (analysis of variance) was used for comparison using SPSS 11.0J (Tokyo, Japan). TEd (5 ms), TEd (10–20 ms) and TEd (90–100 ms) were the mean threshold reductions at or between the specific

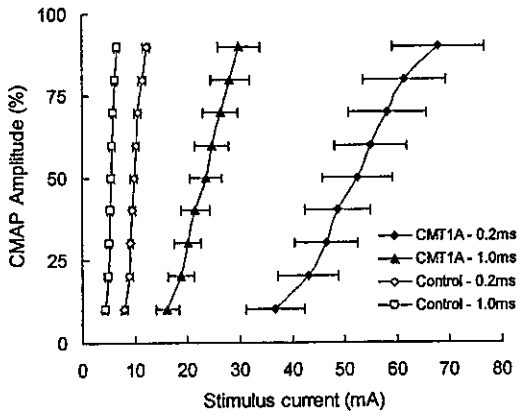

Fig. 1 Absolute stimulus–response curves (mean ± SEM) of median motor axons at the wrist in 53 healthy controls and nine CMT1A patients for two stimulus durations (0.2 and 1.0 ms). The threshold currents were significantly higher and the slopes of the curves were reduced, with greater variability of thresholds, in the patient group.

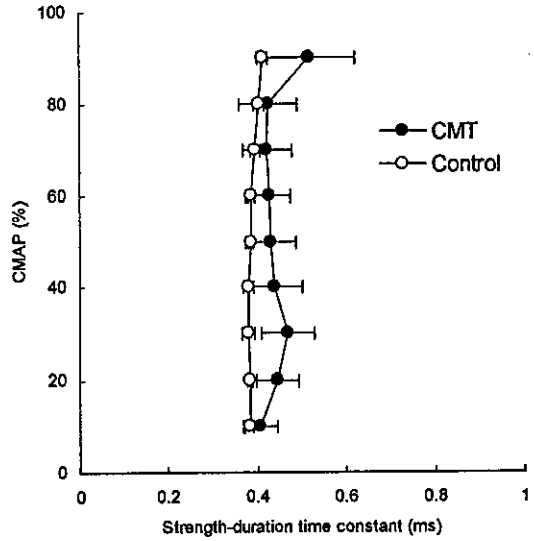

Fig. 2 The strength–duration time constant in CMT1A patients and controls (mean ± SEM). Although the strength–duration time constant was slightly longer in CMT1A than in controls, no significant change was demonstrated.

latencies after the onset of depolarizing current, and TEh (10–20 ms), TEh (20–40 ms) and TEh (90–100 ms) were the corresponding threshold changes after the onset of hyperpolarizing current. TEd (16 ms) – TEd (5 ms) was the difference in the threshold reductions at the respective latencies.

Results

Clinical features and nerve conduction study

Clinical profiles of the patients are shown in Table 1. Electrophysiological features showed diffuse demyelinative sensorimotor polyneuropathy with uniform conduction slowing, typical of CMT1, in all the subjects (Birouk *et al.*, 1997). Note that the median CMAP amplitudes were normal in 66% of the patients. As expected, there was an inverse relationship between age and median CMAP amplitude ($r = -0.61$, $y = -0.0637x + 7.9344$), but otherwise no age effect was observed in the analyses described below.

It has been shown that serum potassium level significantly affects axonal excitability (Kiernan *et al.*, 2002*a*; Kuwabara *et al.*, 2002*b*); the level was obtained in six of the nine subjects and all values were within normal limits (mean 4.1 mEq/l, range 3.7–5.3 mEq/l, normal, 3.5–5.5 mEq/l). As there was no significant change in the parameters assessed below between those from all the CMT patients and from patients with normal serum potassium levels, the remaining statistical analyses compared all the CMT patients with the controls.

Multiple excitability measures using threshold tracking

Stimulus–response curves

In the stimulus–response curves, the threshold currents in the nine CMT1A patients were significantly higher than those in the 53 healthy controls (Fig. 1). The stimulation current required to produce a minimal (10%) CMAP in the CMT1A patients was more than three times as high as that required to produce a maximal CMAP in healthy controls (Fig. 1). To produce a CMAP 40% of maximum, the mean absolute current for the 0.2 ms test stimulus was 48.7 ± 18.8 mA in the CMT1A patients and 9.5 ± 0.6 mA in the controls ($P < 0.001$). The mean absolute current for the 1.0 ms test stimulus was 21.5 ± 8.2 mA in the patients and 5.3 ± 0.5 mA in the controls ($P < 0.001$). Despite the significantly greater stimulation current in the patients, the test was well tolerated by the patients, possibly because of impaired sensation.

Strength–duration properties

Although the strength–duration time constant was slightly increased in the CMT group, there was no significant difference between the two groups (Fig. 2). The strength–duration time constant was fairly stable in both controls and CMT1A patients throughout the different CMAP amplitude levels. However, in CMT1A patients, an inverse relationship between the maximum CMAP amplitude and the strength–duration time constant at the 50% maximum CMAP level ($r = -0.51$) was found.

Recovery cycle

The patterns of the recovery cycles were similar in controls and CMT patients, the relative refractory period lasting <3 ms, supernormality being maximal at the 5-ms conditioning–test interval and late subnormality maximal at ~40 ms (Fig. 3). The extent of the changes in threshold during the refractory period was significantly greater in the control group at the 2-

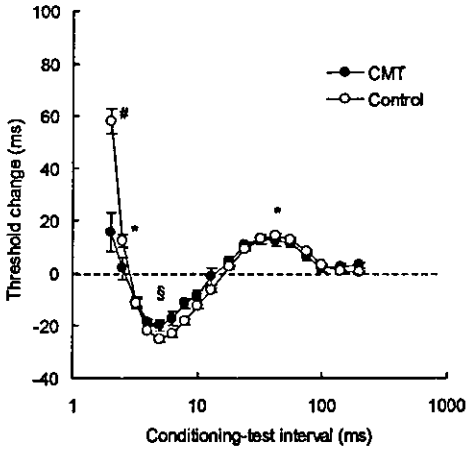

Fig. 3 The recovery cycle in CMT1A patients and controls (mean ± SEM). Nerves from patients with CMT1A showed less pronounced threshold changes in relative refractory and supernormal periods than controls, though durations of each period were similar. $P < 0.0007$; $^{\S}P < 0.02$; *not significant.

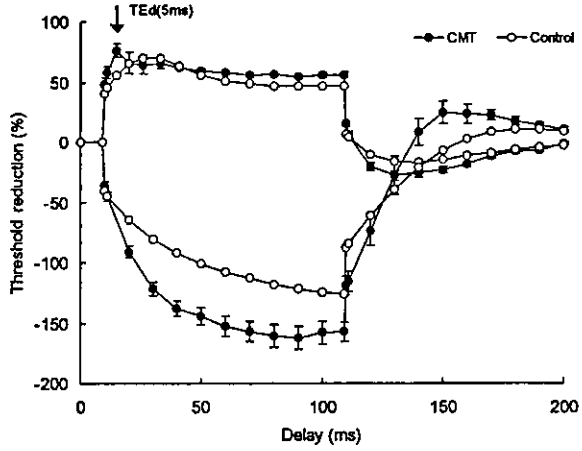

Fig. 4 Threshold electrotonus (mean ± SEM). In CMT1A patients, accommodation to depolarizing currents was stronger and occurred earlier than in controls. There was generalized widening out of the curves in CMT1A (fanning out) and greater accommodation to long hyperpolarizing currents.

ms conditioning–test interval ($P < 0.0007$), but not significantly different at the 2.5-ms interval ($P = 0.10$). For supernormality, the control group demonstrated a greater threshold change than the CMT group ($P < 0.02$), but there was no difference in late subnormality ($P = 0.88$) (Fig. 3). These findings of normal durations of the periods and reduced threshold changes in the patient group compared with those in controls are similar to the data in chronic inflammatory demyelinating polyneuropathy (Cappelen-Smith *et al.*, 2001).

Threshold electrotonus and current–voltage relationships

The most striking abnormalities in excitability parameters were revealed by the recordings of TE (Fig. 4). Table 2 documents comparisons of various excitability measures. Significant changes were observed in the responses to hyperpolarizing current. These were most pronounced in the early part of the responses [TEh (10–20 ms) and TEh (20–40 ms)] (Table 2) but still present at 90–100 ms. A closer look at the early part of the response to depolarizing current [TEd (10–20ms)] also disclosed steeper than normal changes. Because families of these electrotonus response curves can resemble the ribs of a Japanese fan, coming from a point near the origin of the plot (Fig. 6B), these changes can be described as a 'fanning-out' of the responses (Kaji, 1997). The more pronounced curvature in the CMT hyperpolarizing electrotonus suggests more accommodation due to activation of inward rectification by the hyperpolarization-activated current I_H (see Discussion).

The depolarizing electrotonus was more complicated, the CMT patients exhibiting first more, then less, and then more threshold reduction than the controls. At 5 ms, the depolarizing current induced a significantly greater threshold reduction than in controls (fanning-out). This was, however, quickly followed by an accommodative fall in threshold, between 5 and 16 ms. At longer delays, the CMT patients again showed a significantly greater threshold reduction than controls.

The current–threshold relationship (Fig. 5) also showed evidence of contrasting changes in passive and voltage-dependent membrane properties. With small currents, the slope of the current–threshold relationship was reduced, which, like the early fanning out of the TE, indicates that a greater fraction of the applied current was reaching the internodal axon (see Discussion). With larger currents, however, the slope was increased, in both the depolarizing and hyperpolarizing directions, until the absolute threshold changes returned towards and crossed the control curves respectively, indicating increased outward and inward rectification. Neither the TE nor the current–threshold relationship revealed correlation between CMAP amplitude and the extent of the nerve excitability abnormalities.

Discussion

The present study has shown that, in CMT1A, recognized as a polyneuropathy with uniform demyelination, there are consistent changes in nerve excitability properties, especially in resting thresholds and in TE. These changes were unlikely to be related to axonal degeneration, as CMAP amplitudes were fairly well preserved in the tested nerves, and there was no correlation between CMAP amplitude and the extent of the electrotonus abnormalities. Here we will consider the likely biophysical basis of the excitability changes observed.

Table 2 *Comparison of various excitability measures in TE*

	CMT1A (mean ± SD)	Control (mean ± SD)	*P*
TEd (10–20 ms)	65.5 ± 17.0	68.6 ± 4.9	0.73
TEd (90–100 ms)	56.1 ± 6.0	46.9 ± 4.8	< 0.001
TEh (10–20 ms)	−106.4 ± 15.2	−72.5 ± 6.5	< 0.001
TEh (20–40 ms)	−133.0 ± 16.3	−91.0 ± 10.6	< 0.001
TEh (90–100 ms)	−157.1 ± 25.7	−125.3 ± 24.1	< 0.004
TEd (5 ms)	76.2 ± 16.7	56.2 ± 3.7	< 0.001
TEd (16 ms) − TEd (5 ms)	−11.5 ± 23.9	14.0 ± 3.2	< 0.001

Values are threshold reduction (%).

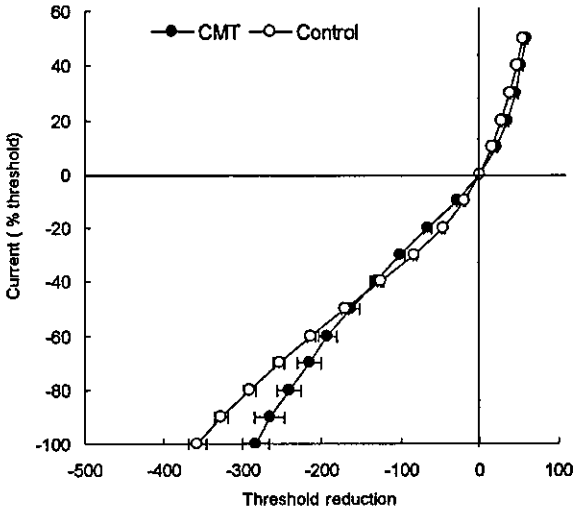

Fig. 5 The current–threshold relationship (mean ± SEM) demonstrated no statistical difference between the CMT1A and controls. However, the CMT group had a tendency to have greater threshold changes to depolarizing and weak hyperpolarizing currents consistent with fanning out in TE, and smaller changes in response to strong hyperpolarizing currents.

Increased resting threshold and early fanning out of threshold electrotonus

Figure 6 shows a simplified equivalent circuit for a segment of axon (node + internode), which accounts for the fast and slow phases of electrotonus and threshold (Barrett and Barrett, 1982; Yang *et al.*, 2000). It shows how an applied current (I) is divided into two components, a nodal component (I_n), which alters the potential on the nodal membrane by an amount I_nR_n (Ohm's law), and an internodal component (I_i), which initially changes the potential on the internodal axolemma at the rate I_i/C_i (as $C_i = I_i * t$). The initial proportion of current that crosses the nodal membrane (I_n/I) is set by the resistance ratio $R_{il}/(R_{il} + R_n)$, whereas the proportion crossing the internodal membrane (I_i/I) is $R_n/(R_{il} + R_n)$. The substantial increase in resting threshold current, and the increase in the early fanning out of TE indicate that in CMT1A the proportion of applied current crossing the nodal membrane is decreased and the proportion crossing the internodal membrane is correspondingly increased, i.e. that R_{il} is reduced in relation to R_n. If R_n were increased, the current threshold would fall, so we conclude that there is a reduction in R_{il}, which could be caused either by thin or 'leaky' myelin, or by a loosening of the axon–Schwann cell paranodal seal; both of these changes are consistent with the pathology of CMT1A. The reduction in R_{il} reduces I_n/I, so that the applied current has to be increased to reach the same threshold depolarization of the node. The reduction in R_{il} also increases I_i/I and the initial rate of polarization of the internodal axolemma. In a previous paper we introduced the idea of the 'fan' origin of TE (Bostock 1995; Kaji 1997; Yang *et al.*, 2000): the point (found by projecting back the tangents to the initial portion of slow electrotonus to the resting threshold) from which the slow electrotonus appears to originate (O in Fig. 6B). The time interval (t_f) from the fan origin to the time of current application was shown to be $C_iR_{il}(R_{il} + R_n)/R_n$ for the simplified circuit of Fig. 6A. A reduction in R_{il} reduces t_f and causes a more acute fanning-out of electrotonus.

Increased inward rectification in CMT1A

On the hyperpolarizing side, the early increased fanning out of TE in CMT1A is not maintained (Yang *et al.*, 2001). Inward rectification, most likely due to the slowly activating hyperpolarization-activated current I_H, sets in, so that by 100 ms the CMT1A and control curves are approaching each other, and by 200 ms (the time used for the current–threshold measurements in Fig. 5) the curves cross over for hyperpolarizing currents in excess of 40% of threshold. Greater activation of I_H during hyperpolarization TE in CMT1A patients is also indicated by the excitability overshoot after the end of the hyperpolarizing current at 150 ms, since I_H deactivates slowly. Although the TE and current–threshold data thus both indicate increased activation of I_H in CMT1A patients relative to normal controls, it is not clear whether this implies any alteration in axonal channel function (e.g. channel density). Because threshold currents are abnormally high in CMT1A, the polarizing currents used in the TE and current–threshold recordings are also abnormally high, so that the degree of hyperpolarization of the internodal axon must be much greater. It is therefore quite possible that the increased activation of I_H in CMT1A patients simply reflects

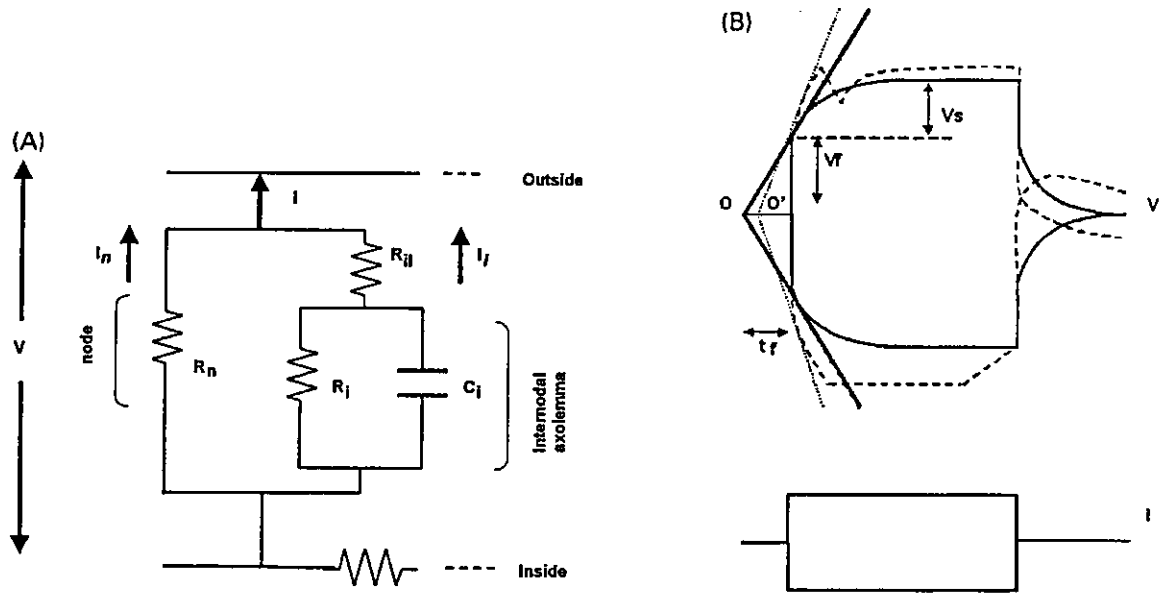

Fig. 6 A mathematical model of TE based solely on passive membrane properties. (**A**) A simplified equivalent circuit of myelinated axon (passive components only) (Barrett and Barrett, 1982), which generates fast and slow components of electrotonus. R_n, nodal resistance; R_{il}, internodal leakage resistance (access resistance to internodal axolemma, through and under the myelin sheath); R_i and C_i, resistance and capacitance of internodal axon. (**B**) Electrotonic changes in membrane potential (V) to long current pulses (I) predicted by the circuit in (**A**) in controls (solid lines) and CMT1A (dashed lines). V_f and V_s, fast and slow components of electrotonus; O and O′, apparent origins of fanning determined by lines tangential to the initial parts of the slow component; t_f, the time from O and O′ to the start of the current pulses. Note that the t_f is shorter in CMT1A than that in controls.

this increased membrane hyperpolarization rather than any abnormality in ion channels.

Rapid outward rectification in CMT1A

On the depolarizing side, the early increased fanning out of TE in CMT1A is much shorter-lived and quickly gives way to rapid accommodation. This rapid accommodation is similar to that previously seen in young rats, which was shown to be due to activation of fast K^+ channel channels that were blocked by 4-aminopyridine (Yang *et al.*, 2000). Whereas in normal, mature myelinated axons the fast K^+ channel channels $K_v1.1$ and $K_v1.2$ are concentrated in the juxtaparanodal region of the internode (Vabnick *et al.*, 1999; Girault and Peles, 2002), where they only affect slow components of electrotonus, in CMT1A they are activated rapidly by applied currents, either because they have spread to the nodal region, or because disruption of the axon–Schwann cell paranodal seal allows more current to reach the juxtaparanodal zone. Prior observations in the experimental demyelination demonstrated similar participation of the internodal K^+ channel channels to action potentials, in accordance with the present findings (Bostock *et al.*, 1981; Brismar, 1981; Chiu and Ritchie, 1981). An alternative viewpoint, suggested by the resemblance of TE in CMT1A patients to that in immature rats (Yang *et al.*, 2000), is that overproduction of the myelin protein PMP22 in the disease may inhibit normal nodal maturation. This interpretation is in accordance with studies demonstrating that axonal cytoskeleton in CMT1A is similar to those in immature axons (Sahenk *et al.*, 1999*b*), and that PMP22 overexpression in mice causes dysmyelination (Robaglia-Schlupp *et al.*, 2002).

Is membrane potential altered in CMT1A?

One of the aims of this study was to test for changes in axonal membrane properties which might be related to secondary axonal degeneration, such as membrane depolarization. Our recordings provide no evidence that membrane potential is appreciably abnormal in CMT1A. It might be argued that the raised thresholds and fanning out of TE are characteristics of membrane hyperpolarization. However, the early fanning out in CMT1A patients is very different from the fanning out seen in hyperpolarization, whether caused by DC currents, release of ischaemia, hypokalaemia or occurring in multifocal motor neuropathy (Kiernan and Bostock, 2000; Kiernan *et al.*, 2002*b*; Kuwabara *et al.*, 2002*b*), in which the deviation from normal increases during 100 ms hyperpolarization. In all of these examples of membrane hyperpolarization, superexcitability was increased relative to normal and relative to the late subexcitability. In CMT1A, however, the recovery cycle is relatively normal (Fig. 3), although refractoriness and superexcitability are significantly reduced. These changes in the recovery cycle are difficult to interpret in the presence of the substantial changes in passive membrane properties, but